Lateral Load Tests of Unbonded Post-Tensioned Precast Concrete Walls

by F. J. Perez, S. Pessiki, R. Sause, and L.-W. Lu

Synopsis:

This paper reports on the experimentally and analytically observed behavior of unbonded post-tensioned precast concrete walls under static monotonic and cyclic lateral loads. Results show that the limit states that characterize the lateral load behavior of the walls occur as anticipated in the design of the walls and at force and drift levels predicted by the analytical model, except that the experimentally observed drift capacity exceeds the drift capacity predicted by the analytical model. Cyclic lateral load results show that unbonded post-tensioned precast walls can undergo significant nonlinear lateral drift without significant damage, and can maintain their ability to self-center, thus eliminating residual lateral drift.

Keywords: concrete; earthquake; precast; prestressed; seismic; unbonded; walls

ACI Member Felipe J. Perez is a Ph.D. candidate in the Department of Civil and Environmental Engineering at Lehigh University. He received his B.S. from California State University, Northridge and his M.S. from Lehigh University. His research interests include the seismic evaluation of prestressed concrete structures.

ACI Member Stephen Pessiki is an Associate Professor of structural engineering at Lehigh University. He is Secretary of ACI Committee 228, Nondestructive Testing of Concrete. His research interests include nondestructive evaluation of structures and the behavior and design of reinforced and prestressed concrete structures.

ACI Member Richard Sause is a professor of structural engineering and Director of the Center for Advanced Technology for Large Structural Systems (ATLSS) at Lehigh University. He was a co-recipient of the ACI Structural Research Award in 1987. His research interests include the behavior, design, and analysis of reinforced concrete; precast concrete; and concrete composite structures under earthquake loading.

Le-Wu Lu is the Bruce G. Johnston Professor of structural engineering at Lehigh University. He has conducted extensive research in seismic behavior and design of reinforced concrete, steel and composite structures. He is an active ACI member.

INTRODUCTION

Past earthquakes have demonstrated the superior seismic performance of buildings with reinforced concrete walls as the primary lateral load resisting system (1). However, the provisions of current U.S. building codes limit the use of precast concrete walls as a primary lateral load resisting system in seismic regions. Precast concrete systems that can be designed in the U.S. under current building codes use connections made with cast-in-place concrete, resulting in precast walls that emulate cast-in-place walls. However, these emulative precast walls do not have all the economic advantages of precast construction as a result of the cast-in-place concrete and expensive details in the connections.

Alternative non-emulative precast seismic structural systems have been developed that take advantage of natural discontinuities at the connections of precast systems. In the U.S., these alternative systems have been the focus of the PRESSS (PREcast Seismic Structural Systems) program, initiated in 1990. PRESSS research has shown that the unbonded post-tensioned connections of

precast elements result in precast systems with excellent load-deformation hysteretic behavior (2, 3, 4). An analytical study of the seismic response of unbonded post-tensioned precast concrete walls with horizontal joints was carried out at Lehigh University by Kurama et al. (5). These unbonded post-tensioned precast walls are constructed by post-tensioning precast wall panels across horizontal joints at the floor levels (Figure 1). Grout is used between the joints for construction tolerances. The analytical study shows that, as a result of unbonding, large nonlinear lateral drifts can be achieved in a wall without yielding or fracturing the post-tensioning steel. Dynamic analysis results indicate that unbonded post-tensioned precast walls have large flexural ductility and self-centering capacity without sustaining significant damage and excessive drift under moderate-to-severe earthquakes.

An experimental program to verify the results of this analytical study is underway at Lehigh University. This paper discusses the behavior of unbonded post-tensioned precast concrete walls subjected to static monotonic and cyclic lateral loads. The experimental results obtained to date are compared with results obtained using the analytical model developed by Kurama et al. (5).

RESEARCH SIGNIFICANCE

Current U.S. building provisions limit the use of precast concrete walls as a primary lateral load resisting system in seismic regions. It has been shown that the use of unbonded post-tensioned connections of precast elements results in precast systems with excellent load-deformation hysteretic behavior (2, 3, 4). Dynamic analysis results indicate that unbonded post-tensioned precast walls have large flexural ductility and self-centering capacity without sustaining significant damage and excessive drift under moderate-to-severe earthquakes (5). However, the experimental data necessary to verify the analytical model used in the dynamic analyses was not previously available. This paper presents experimental data on unbonded post-tensioned precast concrete walls under static monotonic and cyclic lateral loads and compares the results with analytical results based on the model used in Ref. 5.

EXPECTED LATERAL LOAD BEHAVIOR

The walls considered in this study are shown schematically in Figure 1. Each wall is comprised of six one-story-tall precast panels that are connected along horizontal joints using unbonded post-tensioned steel, which is anchored at the roof and within the foundation (Figure 1(a)). Interlocking spirals are used to confine the concrete at the ends of the base panel, as shown in Figure 1(b). This confinement (which can alternatively consist of hoop reinforcement, as discussed

later) enables the base panel to sustain the large compressive strains that develop as a result of gap opening displacements that occur along the base of the wall due to lateral loads.

As shown in Figure 2, the lateral load behavior of unbonded post-tensioned walls is characterized by several limit states: (1) decompression at the base of the wall, denoted by the symbol (■); (2) effective limit of the linear-elastic response of the wall, denoted by the symbol (●); (3) yielding of the post-tensioning steel, denoted by the symbol (×); (4) base shear capacity; and (5) crushing of confined concrete, denoted by the symbol (▲). The limit states are described below.

Decompression at the base of the wall occurs when the precompression due to post-tensioning at one end of the base of the wall is reduced to zero by the overturning moment. Under a specified lateral load distribution, decompression of the wall can be related to a specific level of base shear and lateral drift, V_{dec} and Δ_{dec} respectively. Decompression is accompanied by the *initiation* of gap opening along the horizontal joint between the base panel and the foundation.

The point on the base-shear-lateral-drift response of a wall corresponding to the effective limit of the linear-elastic response is called the effective linear limit. This limit state denotes the onset of a substantial reduction in lateral stiffness (called softening), which is caused by significant gap opening along the horizontal joint between the base panel and the foundation. The base shear and lateral drift corresponding to the effective linear limit are denoted as V_{ell} and Δ_{ell} respectively. Softening usually occurs in a smooth and continuous manner in a precast wall with unbonded post-tensioned horizontal joints (5). Hence, the term *effective* linear limit is used to describe this point on the base-shear-lateral-drift relationship.

Yielding of the post-tensioning (PT) steel occurs when the strain in the steel reaches the linear limit. The base shear and lateral drift corresponding to the linear limit strain of the outermost PT steel are denoted as V_{llp} and Δ_{llp} respectively. Since the PT steel is unbonded, this limit state is reached after a large lateral drift has occurred, providing the wall with significant drift capacity before inelastic deformation develops in the PT steel (5).

Failure of the wall occurs when the confined concrete at the base of the wall fails in compression. Thus, the drift capacity of the wall is controlled by the compression strain capacity of the confined concrete. Figure 1 shows spiral confined concrete, although other confining reinforcement details may be used. The base shear and lateral drift corresponding to failure of the confined concrete are denoted as V_{ccc} and Δ_{ccc} respectively. In a well-designed wall Δ_{ccc} is significantly larger than Δ_{llp}. Also, the base shear capacity of the wall is V_{llp}, which is approximately equal to V_{ccc}. Thus, in a well-designed wall, the base shear capacity is governed by the axial-flexural (overturning) capacity of the wall, rather than the shear sliding capacity.

EXPERIMENTAL PROGRAM

An experimental program is underway in the Center for Advanced Technology for Large Structural Systems (ATLSS) at Lehigh University to study the behavior of isolated multi-story unbonded post-tensioned precast concrete walls with horizontal joints under static monotonic and cyclic lateral loads. Figures 3(a) and 4(a) show the properties of the full-scale wall considered in this study. The full-scale wall was scaled by a factor of 5/12 (except for the thickness which was scaled by a factor of 1/2 so that the wall cross-section could accommodate the reinforcing steel and cover concrete). The properties of the scaled wall are shown in Figures 3(b) and 4(b). Due to laboratory height restrictions, the wall specimens tested in the laboratory (i.e., test walls) consider only the bottom four stories of the scaled wall. The test walls are described next.

An elevation of the test walls is shown schematically in Figure 3(c). Each test wall is comprised of four wall panels, a loading block, and two extension panels. The test wall rests on a precast concrete foundation, which has a manhole to access the inside of the foundation, where the unbonded PT bars (shown dashed) are anchored. The four wall panels of the test wall represent the bottom four panels of the scaled wall (see Figures 3(b) and 3(c)). The bottom two panels of the test wall have special confining reinforcement on both ends, as shown by the shaded regions in Figure 3(c). The cross-section of the bottom two panels of the test wall is the same as the cross-section of the base panel of the scaled wall (Figure 4(b)). It is noted that the confinement in the second panel of the test wall is provided to preserve the panel's integrity and thus make it reusable throughout the test program.

The loading block, which rests on the fourth panel, is used to apply gravity and lateral loads. The gravity load is applied by stressing an external bar on each side of the wall using a hydraulic cylinder. The gravity load remains essentially constant throughout the experiment. The lateral load actuator is connected to the loading block at a height of 7.23 m (23.73 ft.) from the base of the wall. This height represents the resultant of a triangular inertia force profile with zero load at the base and the maximum load at the roof (Figure 3(b)). The lateral load actuator, acting at the resultant of the triangular inertia force profile, generates the same moment to shear ratio at the base of the test wall as does the triangular inertia force profile on the scaled wall. The two extension panels above the loading block help provide a total unbonded height of 9.91 m (32.50 ft.), which is the unbonded height of the scaled wall.

As noted above, the experimental program is designed to study the lateral load behavior of isolated multi-story unbonded post-tensioned precast concrete walls with horizontal joints. In a building, a wall is restrained from out-of-plane motion by the surrounding structural elements. Therefore, to study the behavior of isolated walls in the laboratory, a bracing frame was designed to brace the test

walls against out-of-plane movement. To ensure that the test walls are properly braced during the tests, as the walls displace laterally, and to significantly reduce the lateral forces transmitted to the bracing frame, the following bracing method is implemented. Four steel plates are attached to each wall panel (two on each side) at approximately 20 cm (8 in.) below the top of each panel. The loading block has two steel plates attached to it (one on each side) at the centerline of the wall, just below the pocket where the gravity load actuators rest (see Figure 3(c)). Each of the steel plates has a Teflon pad epoxied to it on the exposed face. The Teflon bracing pads, which move with the test walls, slide against the machined flanges of guide beams located near the wall horizontal joints. The sliding of Teflon on steel reduces the amount of lateral load transferred from the test wall onto the bracing frame through friction. It is noted that at the time the bracing pads are grouted to the panels, gaps between 0.79 mm (1/32 in.) and 1.59 mm (1/16 in.) are left between the Teflon and the machined flange surfaces along the height so that the walls are completely isolated under their own self weight.

The effect of four parameters on the flexural behavior of the walls is investigated by the experimental program. As summarized in Table 1, these parameters are: (1) total area of post-tensioning steel across a horizontal joint, A_p; (2) initial stress in post-tensioning steel, f_{pi} (normalized with respect to the ultimate strength of the post-tensioning steel, f_{pu}); (3) initial stress in concrete due to post-tensioning, $f_{ci,p}$; and (4) confining reinforcement details in the base panel. To date, test walls TW1 and TW2 have been tested to compare the effects of monotonic versus cyclic loading on the flexural behavior of the walls.

TEST WALL ANALYTICAL MODEL

The test wall (shown schematically in Figures 3(c) and 4(b)) is modeled using the DRAIN-2DX program (6). Analytical modeling of unbonded post-tensioned precast concrete walls using the DRAIN-2DX program is described in detail in Ref. (7). The analytical model requires discretized uniaxial stress-strain curves for confined and unconfined concrete and a bi-linear stress-strain curve for the unbonded PT steel. The stress-strain curve for the unconfined concrete was obtained by testing unconfined concrete cylinders. The cylinders were tested shortly after the test walls were tested, and thus represent the stress-strain relationship at the time of testing.

The confined concrete stress-strain relationship was obtained by testing a stub-panel in compression. The stub-panel was taken from the confined region on the tension side of the base panel of wall TW1. This portion of the wall was undamaged when wall TW1 was tested under a monotonic lateral load. Details of the stub-panel test are found in Ref. (8).

The stress-strain relationship of the PT bars was obtained by testing samples taken from PT bars that did not yield during the testing of wall TW1.

RESULTS AND DISCUSSION

This section presents the experimental and analytical results obtained for two test walls, TW1 and TW2. Wall TW1 was tested under a static monotonic lateral load, while wall TW2 was tested under a static cyclic lateral load.

Monotonic Test Results (TW1)

Figure 5 shows the monotonic lateral load results obtained experimentally and analytically for wall TW1. The base shear corresponds to the lateral load applied by the horizontal actuator shown in Figure 3(c). The lateral drift is taken as the horizontal displacement at the level of the actuator, divided by the height of the actuator relative to the base of the wall (i.e., 7.23 m (23.73 ft.)). The smooth plot in Figure 5 is obtained analytically using the wall model discussed above. The plot with the repeated load drops is the experimental result. Each load drop is a result of a temporary halt in the loading of the specimen.

Comparing Figure 5 to Figure 2, it can be seen that the lateral load behavior of the wall corresponds well with the expected behavior, which (as discussed earlier) is characterized by the limit states of decompression, the effective linear limit, yielding of the PT steel, and crushing of the confined concrete. Figure 6 shows that, as anticipated, the lateral load behavior of an unbonded post-tensioned wall is accompanied by a large gap opening along the base panel-to-foundation connection, which develops as the precompression due to prestressing is overcome by the overturning moment due to lateral load. This maximum measured gap opening was 7.26 cm (2.86 in.), corresponding to the peak lateral drift of 3.57%.

Figure 5 also shows that (except for the lateral drift at failure) there is an excellent correlation between the wall analytical model and the experimental result. The results obtained for various limit states from the analytical model and the experiment of wall TW1 are summarized in Table 2.

The difference in the lateral drift at failure (i.e., lateral drift corresponding to crushing of confined concrete, Δ_{ccc}) suggests that the compressive strain demand in the concrete, as a function of the lateral drift of the wall, may be smaller in the experiment than in the analytical model. That is, the model, which assumes plane sections in the concrete, overestimates the compressive strains at the base of the wall, and thus predicts an early failure when compared to the experiment.

Cyclic Test Results (TW2)

Wall TW2 was tested under a static cyclic lateral load. The wall was subjected to the following drift cycles, controlled by the displacement at the level of the loading block: 3 cycles at 0.05%, 0.1%, 0.25%, 0.5%, 0.1%, 1%, 1.5%, 2%, 0.1%, and one cycle at 3%. The first group of drift cycles (at 0.05%) displaces the wall to a drift that is below Δ_{dec}. The second through fourth groups of drift cycles (at 0.1%, 0.25%, and 0.5%) displace the wall to drifts that are between Δ_{dec} and the Δ_{ell}. The fifth group of drift cycles (at 0.1%) is included to check the initial wall stiffness after the wall has been subjected to the previous four groups of drift cycles. The sixth group of drift cycles (at 1%) displaces the wall to a drift that is between Δ_{ell} and Δ_{llp}. The seventh group of drift cycles (at 1.5%) displaces the wall to a drift that is slightly larger than Δ_{llp}. The eighth group of drift cycles (at 2%) displaces the wall to a drift that is significantly larger than Δ_{llp}, but less than Δ_{ccc}. The ninth group of drift cycles (at 0.1%) is included to check the initial wall stiffness after the wall has been subjected to the previous eight groups of drift cycles. Finally, the last drift cycle at 3% is intended fail the wall as it reaches Δ_{ccc}.

Figure 7 compares the experimental cyclic lateral load results for wall TW2 to the experimental monotonic lateral load results for wall TW1. The results obtained for various limit states are summarized in Table 2 for both walls. Figure 7 and Table 2 show that the lateral load results for the two walls are in good agreement. It is observed in Figure 7 that the monotonic curve for wall TW1 forms an envelope to the cyclic lateral load results for wall TW2.

The cyclic test results show that an unbonded post-tensioned precast concrete wall exhibits a nearly nonlinear elastic load-deformation response with a small amount of energy dissipation per cycle of loading. Before yielding of the post-tensioning steel, the nonlinearity results from gap opening that occurs between the base panel-to-foundation connection. In addition, it can be observed that the wall exhibits excellent self-centering behavior. The self-centering capability of the wall is only slightly compromised when it is loaded past yielding of the PT steel.

Figure 8 compares the analytical cyclic lateral load results for wall TW2 (shown dashed and labeled "TW2-Analytical") to the experimental monotonic lateral load results for wall TW1. The experimental and analytical results obtained for walls TW1 and TW2 for various limit states are summarized in Table 2. Figure 8 and Table 2 show that the results obtained using the analytical model for wall TW2 correlate well with the experimental results obtained for walls TW1 and TW2. The analytical model for wall TW2 (cyclic case) exhibits the same behavior as the experimental test wall subjected to cyclic loading (TW2). Namely, the lateral load behavior is nearly nonlinear-elastic with a small amount

of energy dissipation per cycle of loading. In addition, the analytical model displays the excellent self-centering characteristics observed in the experiment.

Figure 9(a) compares the first cycle of experimental and analytical behavior at 1% drift, 1.5% drift, and 2% drift for wall TW2. The analytical curve is shown dashed. It can be seen that for each cycle of loading, the analytical wall predicts the cyclic behavior quite well. Figure 9(b) compares the first cycle of experimental and analytical behavior at 1% drift, 1.5% drift, 2% drift, and 3% drift for wall TW2. Figure 9(b) shows that the analytical wall reaches the strain capacity in the confined concrete during the first half of the first drift cycle at 3%, while the experimental wall (TW2) failed by crushing of the confined concrete during the second half of the same drift cycle. Therefore, the analytical model was able to predict the lateral load behavior of the experimental test wall quite well up to failure by confined concrete failure. However, it was unable to predict a subsequent failure mode, as discussed next.

FAILURE MODES

An unbonded post-tensioned precast concrete wall that is well designed and adequately detailed is expected to fail when the confined concrete at the base of the wall fails in axial-flexural compression. This failure occurs when the confining steel fractures and the lateral confining pressure in the confined concrete is lost. As noted earlier, the lateral drift when failure of the confined concrete occurs is denoted as Δ_{ccc}. This limit state is shown in Figure 7 for walls TW1 and TW2 and is labeled as "Failure TW1" and "Failure TW2a," respectively. The observed failure at the base of the wall TW1 is shown in Figure 10. Figure 10(a) shows an elevation of the base panel after failure. After excavating the concrete at the base of the compression edge of the wall, it was observed that the spirals fractured in the through-thickness direction of the wall, as shown in Figure 10(b). The same mode of failure was observed for wall TW2 (Failure TW2a), as shown in Figures 11(a) and 11(b).

After Failure TW2a occurred at one end of the wall for the cyclic test (wall TW2), the specimen was loaded in the opposite direction for additional cycles, as shown in Figure 12 until that side of the wall failed (labeled "Failure TW2b"). As shown in Figure 11(c), Failure TW2b was a sudden buckling failure of the confined concrete region of the base panel. It is important to emphasize that only the confined concrete region buckled, while the rest of the base panel did not, as shown in Figure 11(c) by the vertical conduit which remained attached to the unbuckled portion of the panel. This failure mode can be explained as follows. During testing of wall TW2, as the wall was subjected to cyclic lateral loads, numerous short diagonal cracks formed in a narrow vertical band along the height of the base panel. These cracks formed adjacent to the vertical conduit shown in Figure 11(c), which was the outermost conduit, next to the highly

confined region (see also Figure 4(b)). The development of these cracks ultimately permitted the confined concrete region to separate from the rest of the wall. As a result, the confined region, which was carrying significant compressive stresses, buckled after it was no longer restrained from buckling by the rest of the wall. This mode of failure is undesirable as the gravity load capacity of the wall is jeopardized. Consequently, the base panel reinforcement details were modified to better control cracking and to prevent this failure mode. Figure 13 shows the new reinforcement details. The new reinforcement utilizes hoops in the confined region; has horizontal steel that runs the length of the wall and is developed within the confined regions; and has transverse (thru-thickness) hoops adjacent to all conduits to prevent the two layers of horizontal reinforcement from separating relative to one another. These details will be used for the remaining tests, as shown in Table 1. These new reinforcement details are expected to keep the confined concrete region integral with the rest of the base panel to eliminate the buckling failure.

CONCLUSIONS

This paper reports on the experimentally and analytically observed lateral load behavior of unbonded post-tensioned precast concrete walls. The limit states that characterize the lateral load behavior are outlined. Results of monotonic and cyclic lateral load tests of large-scale wall specimens are presented and compared with analytical results. The results show that the limit states that characterize the lateral load behavior occur as anticipated in the design of the walls and at force and drift levels predicted by the analytical model, except that the experimentally observed drift capacity significantly exceeds the drift capacity predicted by the analytical model. The results demonstrate that unbonded post-tensioned precast walls can be designed to undergo significant nonlinear lateral drift without significant damage, and to retain their ability to self-center, thus eliminating residual lateral drift. The cyclic lateral load behavior of the walls is nearly nonlinear elastic, with only a small amount of energy dissipation per cycle of loading. As a result, larger lateral drifts can be expected under earthquake loading. However dynamic analysis results (5) show that these walls can be designed to avoid sustaining excessive drift under moderate-to-severe earthquakes.

ACKNOWLEDGMENTS

This research is funded by the National Science Foundation (NSF) under Grant No. CMS-9612165 as part of the PREcast Seismic Structural Systems (PRESSS) program. The support of NSF program director S.C. Liu is gratefully acknowledged. The research is also supported by the Precast/Prestressed Concrete Institute (PCI) and by the Pennsylvania Infrastructure Technology Alliance through a grant from the Pennsylvania Department of Community and Economic Development. Numerous individuals from the U.S. Precast Concrete Industry have also provided assistance. The opinions, findings, and conclusions in this paper are those of the authors and do not necessarily reflect the views of those acknowledged herein.

REFERENCES

1. Fintel, M., "Performance of Buildings with Shear Walls in Earthquakes of the Last Thirty Years," *PCI Journal*, Precast/Prestressed Concrete Institute, V. 40, No. 3, May-Jun. 1995, pp. 62-80.

2. Cheok, G.; Stone, W.; and Lew, H., "Model Precast Concrete Beam-to-Column Connections Subject to Cyclic Loading," *PCI Journal*, Precast/Prestressed Concrete Institute, Vol. 38, No. 4, Jul.-Aug. 1993, pp.80-92.

3. MacRae, G., and Priestley, M., "Precast Post-Tensioned Ungrouted Concrete Beam-Column Subassemblage Tests," Repost No. PRESSS – 94/01, Department of Applied Mechanics and Engineering Sciences, Structural Systems, University of California, San Diego, CA, Mar. 1994.

4. Priestley, M., and Tao, J., "Seismic Response of Precast Prestressed Concrete Frames with Partially Debonded Tendons," *PCI Journal*, Precast/Prestressed Concrete Institute, Vol. 38, No. 1, Jan.-Feb. 1993, pp. 58-69.

5. Kurama, Y.; Pessiki, S.; Sause, R.; and Lu, L.-W., "Seismic Behavior and Design of Unbonded Post-Tensioned Precast Concrete Walls," *PCI Journal*, Precast/Prestressed Concrete Institute, Vol. 44, No. 3, May-Jun. 1999, pp. 72-89.

6. Prakash, V.; Powell, G.; and Campbell, S., "DRAIN-2DX Base Program Descriptioin and User Guide; Version 1.10," *Report* No. UCB/SEMM-93/17&18, Structural Engineering Mechanics and Materials, University of California, Berkeley, Dec. 1993.

7. Kurama, Y.; Sause, R.; Pessiki, S.; and Lu, L.-W., "Lateral Load Behavior and Seismic Design of Unbonded Post-Tensioned Precast Concrete Walls," ACI Structural Journal, Vol. 96, No. 4, Jul.-Aug. 1999, pp. 622-632.

8. Horan, S., "Materials Modeling for Unbonded Post-Tensioned Precast Concrete Walls," M.S. Thesis, Department of Civil and Environmental Engineering, Lehigh University, Bethlehem, PA, Jan. 2003.

NOTATION

A_p	=	total area of post-tensioning steel across a horizontal joint
ccc	=	crushing of confined concrete state
dec	=	decompression state
ell	=	effective linear limit state
$f_{ci,p}$	=	initial stress in concrete due to post-tensioning
f_{pi}	=	initial stress in post-tensioning steel
f_{pu}	=	post-tensioning steel ultimate strength
llp	=	linear limit of post-tensioning steel state
TW1	=	test wall 1
TW2	=	test wall 2
V_{ccc}	=	base shear at crushing of confined concrete state
V_{dec}	=	base shear at decompression state
V_{ell}	=	base shear at effective linear limit state
V_{llp}	=	base shear at linear limit of post-tensioning steel state
Δ_{ccc}	=	lateral drift at crushing of confined concrete state
Δ_{dec}	=	lateral drift at decompression state
Δ_{ell}	=	lateral drift at effective linear limit state
Δ_{llp}	=	lateral drift at linear limit of post-tensioning steel state

CONVERSION FACTORS

1 in.	=	25.4 mm
1 kip	=	4.448 kN
1 ksi	=	6.897 MPa

Table 1. Parameters studied in experimental program.

Wall	Loading	A_p (cm^2)	f_{pi}/f_{pu}	$f_{ci,p}$ MPa	Confinement Type	Confinement Ratio (%)	
						Volumetric	Area
TW1	monotonic	48.4	0.590	8.20	spirals	7.3	-
TW2	cyclic	48.4	0.590	8.20	spirals	7.3	-
TW3	cyclic	48.4	0.590	8.20	hoops	-	1.75
TW4	cyclic	48.4	0.295	4.10	hoops	-	1.75
TW5	cyclic	24.2	0.590	4.10	hoops	-	1.75

Note: 1 cm^2 = 0.155 $in.^2$; 1MPa = 0.145 ksi.

Table 2. Comparison of experimental to analytical lateral load results.

Wall	Data Type	V_{dec} (kN)	Δ_{dec} (%)	V_{llp} (kN)	Δ_{llp} (%)	Δ_{ccc} (%)
TW1	Experimental	278.3	0.077	687.4	1.342	3.570
TW1	Analytical	230.9	0.077	683.5	1.480	2.634
TW2	Experimental	290.1	0.117	671.0	1.437	2.828
TW2	Analytical	224.0	0.075	701.9	1.540	2.406

Note: 1kN = 0.225 kip.

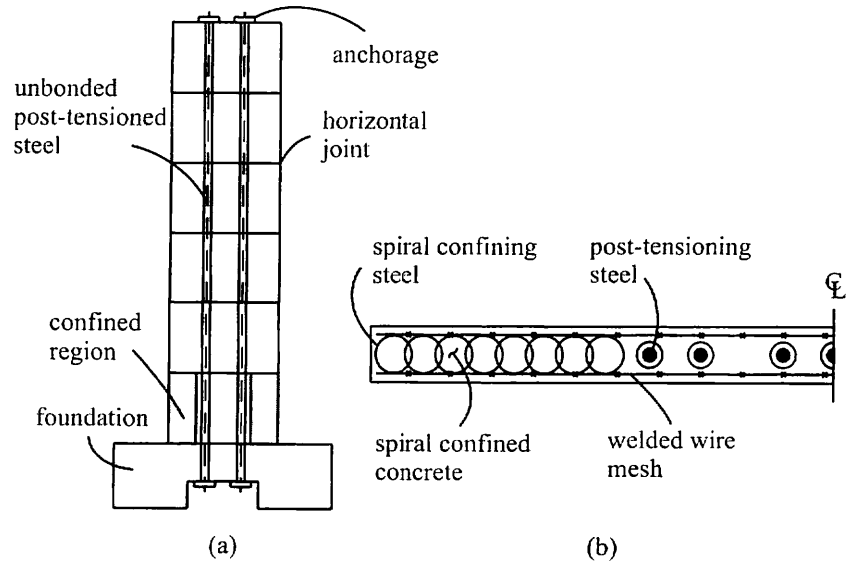

Figure 1. Unbonded post-tensioned wall: (a) elevation view; (b) half of cross-section of base panel.

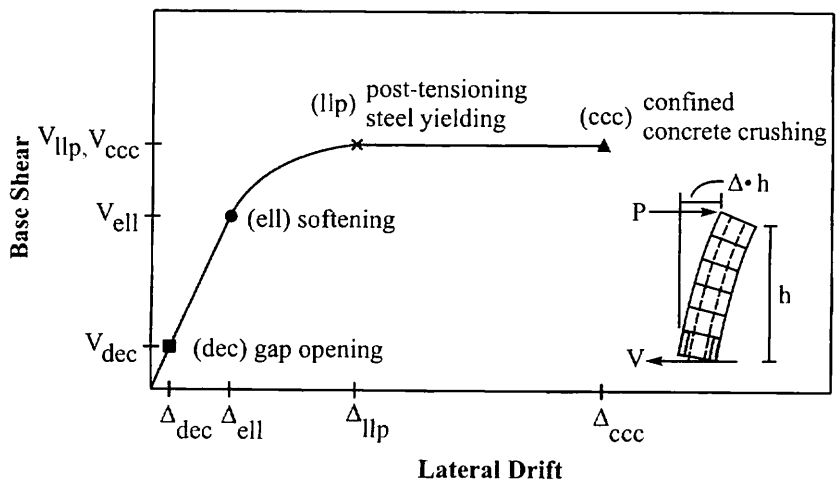

Figure 2. Lateral load behavior of unbonded post-tensioned walls.

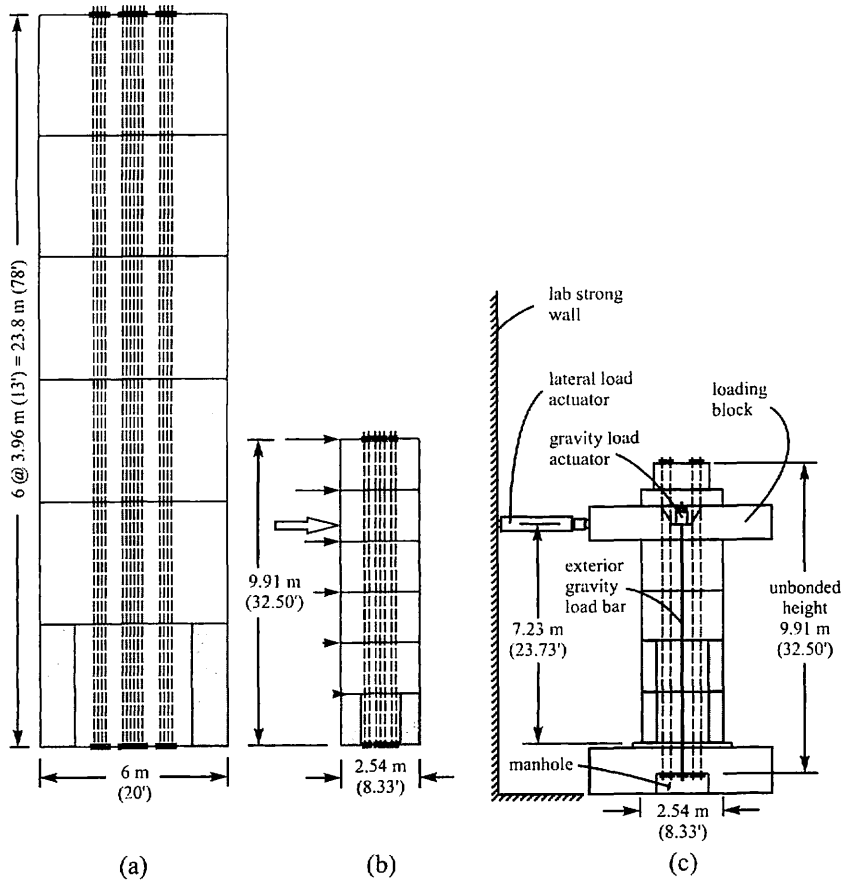

Figure 3. Elevation view: (a) full-scale wall; (b) scaled wall; (c) test wall.

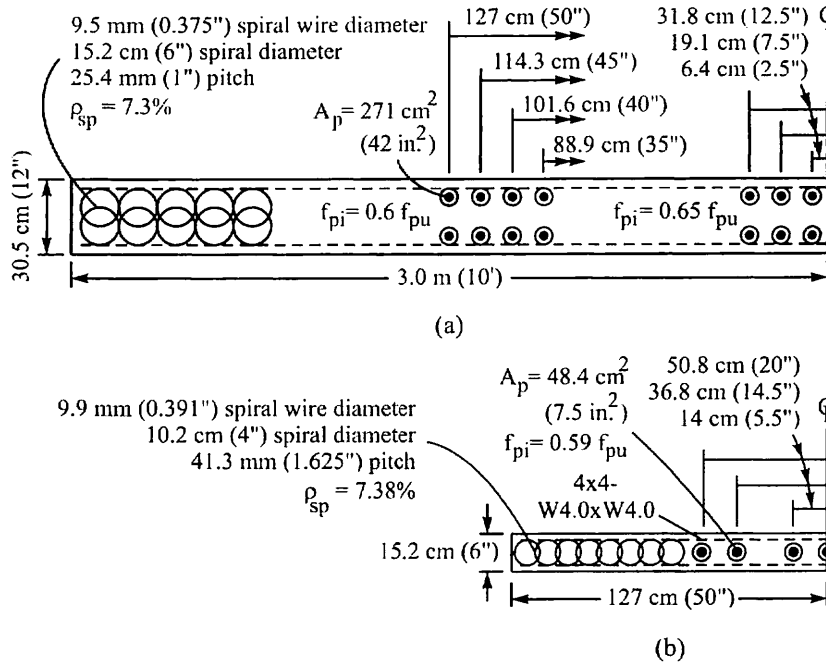

Figure 4. (a) Cross-section at the base of full-scale wall (adapted from Ref. (5)); (b) Cross-section at the base of scaled and test walls.

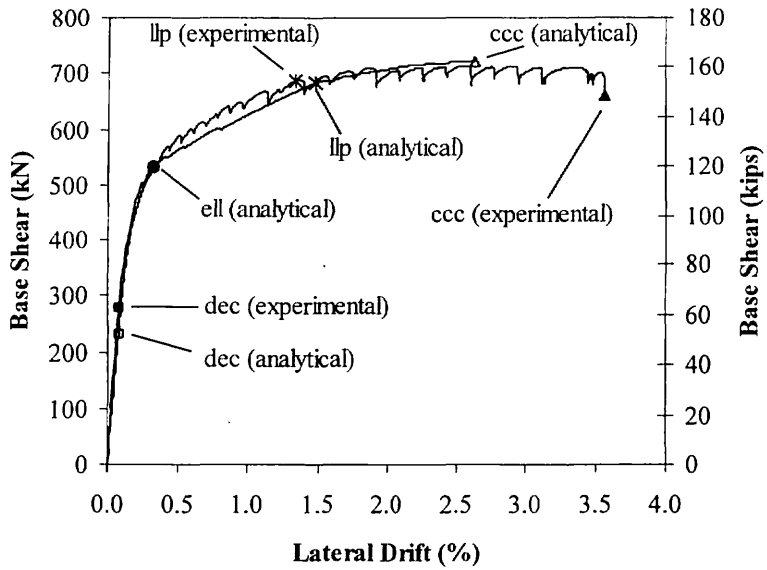

Figure 5. Lateral load behavior of wall TW1.

Figure 6. Gap opening behavior at base of wall TW1 ($\Delta = 3.57\%$).

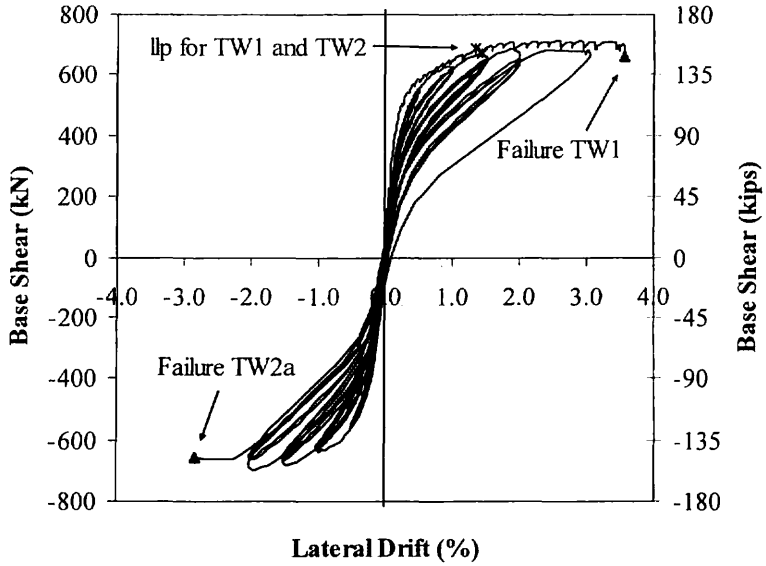

Figure 7. Experimental lateral load behavior of walls TW1 and TW2.

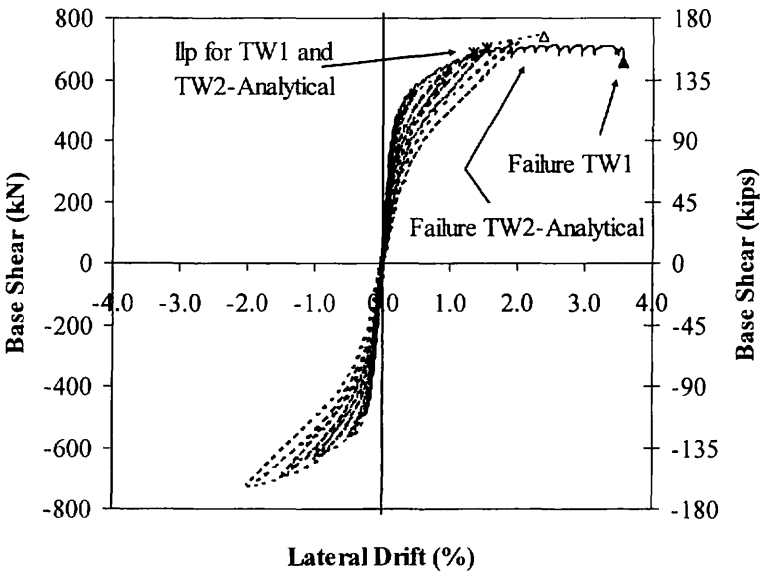

Figure 8. Analytical cyclic behavior of wall TW2.

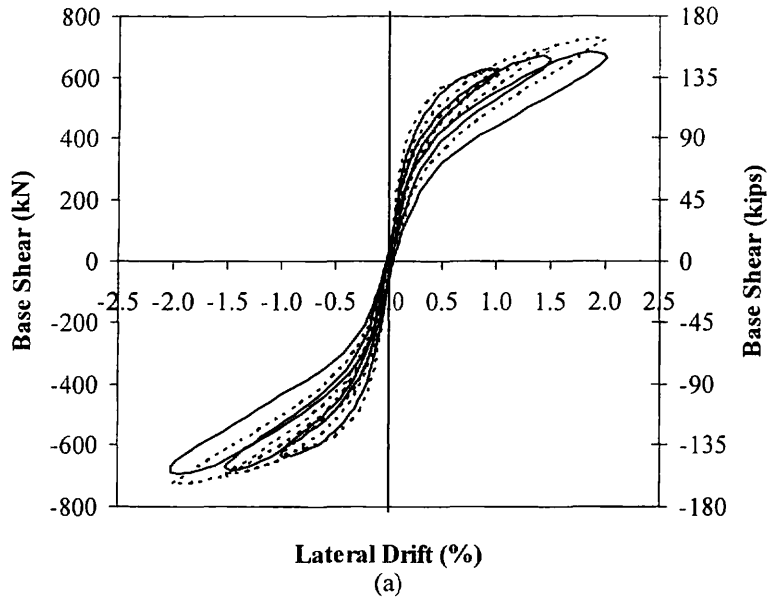

Figure 9. Comparison of analytical to experimental cyclic behavior of wall TW2: (a) first cycle at Δ = 1%, 1.5% and 2%; (b) first cycle at Δ = 1%, 1.5%, 2%, and 3%;

(a)

(b)

Figure 10. Failure mode for wall TW1: (a) failure of confined concrete in base panel (Failure TW1): (b) excavated failure region.

(a)

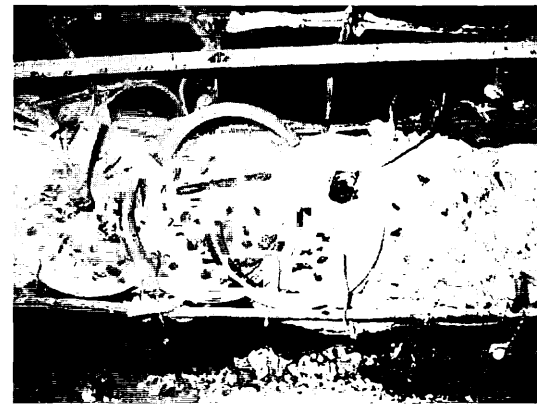

(b)

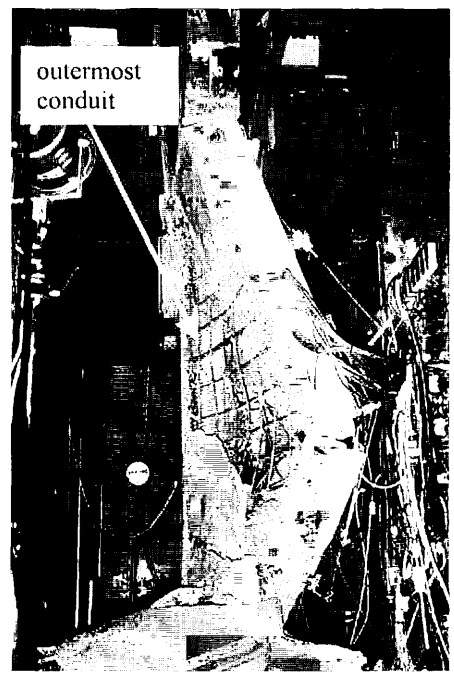

(c)

Figure 11. Failure modes for wall TW2: (a) failure of confined concrete in base panel (Failure TW2a); (b) excavated failure region; (c) instability failure on opposite end of wall (Failure TW2b).

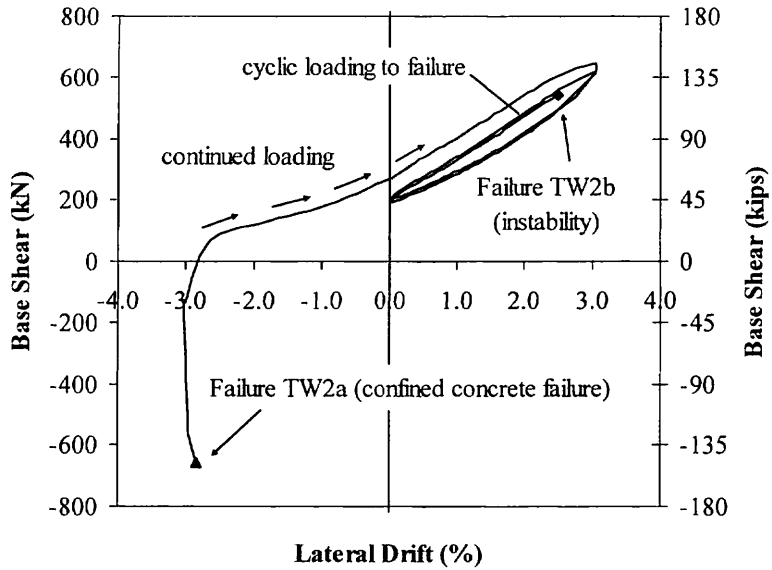

Figure 12. Loading cycles of wall TW2 after Failure TW2a resulting in Failure TW2b.

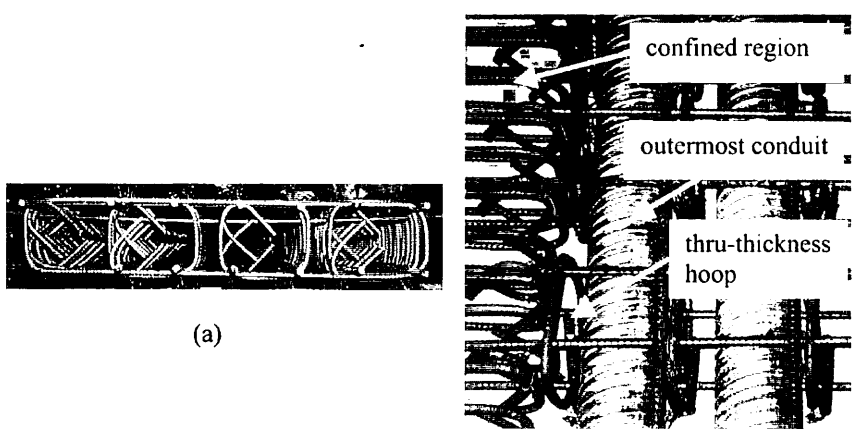

Figure 13. New wall base panel reinforcement details: (a) cross-section of hoop configuration for confined region of walls; (b) details between confined region and region with conduits.